Available online at www.sciencedirect.com

ScienceDirect

Proceedings of the Combustion Institute 35 (2015) 1331–1339

Proceedings of the Combustion Institute

www.elsevier.com/locate/proci

On flame–turbulence interaction in constant-pressure expanding flames

Swetaprovo Chaudhuri [a,b], Abhishek Saha [a], Chung K. Law [a,c,*]

[a] Department of Mechanical and Aerospace Engineering, Princeton University, Princeton, NJ 08544-5263, USA
[b] Department of Aerospace Engineering, Indian Institute of Science, Bangalore 560012, India
[c] Center for Combustion Energy, Tsinghua University, Beijing 100084, China

Available online 16 September 2014

Abstract

In this paper we present one of the first high-speed particle image velocimetry measurements to quantify flame–turbulence interaction in centrally-ignited constant-pressure premixed flames expanding in near-isotropic turbulence. Measurements of mean flow velocity and *rms* of fluctuating flow velocity are provided over a range of conditions both in the presence and absence of the flame. The distributions of stretch rate contributions from different terms such as tangential straining, normal straining and curvature are also provided. It is found that the normal straining displays non-Gaussian *pdf* tails whereas the tangential straining shows near Gaussian behavior. We have further tracked the motion of the edge points that reside and co-move with the edge of the flame kernel during its evolution in time, and found that within the measurement conditions, on average the persistence time scales of stretch due to pure curvature exceed that due to tangential straining by at least a factor of two.

Keywords: Turbulent premixed flame; Stretch rate; High-speed PIV

1. Introduction

An expanding flame is one of the most canonical flame configurations that finds applications spanning from engineering devices like spark-ignition engines to astrophysical events like supernova explosions. Laminar expanding flames have been routinely adopted for experimentally determining laminar flame speeds which is used to (partially) validate chemical reaction mechanisms [1]. All practical flames of this configuration are however turbulent in nature; hence extensive studies have been conducted recently on expanding flames interacting with near-isotropic turbulence [2–13]. The fundamental parameters that quantify the state of turbulence, if it is nearly isotropic, are the turbulence intensity u_{rms} and the integral length scale L_I. The quantities that characterize the local flame structure are the local laminar flame speed $\tilde{S}_L$ and flame thickness δ_L. According to the hydrodynamic theory of premixed flames the stretched laminar flame speed $\tilde{S}_L$ is given by:

$$\tilde{S}_L = S_L - \delta_M \mathbf{K} \tag{1}$$

where S_L and δ_M are the planar laminar flame speed and Markstein length, respectively [14,15],

* Corresponding author at: Mechanical and Aerospace Engineering Department, Princeton University, E-Quad, Olden Street, NJ 08544, USA. Fax: +1 (609) 258 6233.
E-mail address: cklaw@princeton.edu (C.K. Law).

http://dx.doi.org/10.1016/j.proci.2014.07.038
1540-7489/

K is the total stretch rate which can be further decomposed as [16,17]:

$$\mathbf{K} = \overbrace{\underbrace{S_L\kappa}_{\text{stretch rate by pure curvature: } K_c} - \underbrace{(\mathbf{v}\cdot\mathbf{n})\kappa}_{\text{normal strain: } K_n}}^{\text{stretch rate by curvature: } K_\kappa} + \underbrace{\nabla_t\cdot\mathbf{v}_t}_{\text{tangential strain: } K_t}, \quad (2)$$

in which $K_t = (\delta_{ij} - n_i n_j)S_{ij}$, and $\delta_{ij} = 1$ for $i = j$; 0 for $i \neq j$; with S_{ij} being the strain rate tensor. The second and third terms on the RHS of Eq. (2) together is the stretch rate contribution by the strain rate, K_s. Stretch rates originating from the tangential strain rate K_t, normal strain K_n and stretch due to pure curvature K_c can be considered to be parameters that quantify the turbulence–flame interaction as well [18]. In general, turbulence causes multi-scale wrinkling of the flame surface, affecting the aerodynamics of the flame which in turn affects the nearby flow field by heat release and gas expansion. Since the burned products in the expanding flame should be statistically stationary, the flame could induce a mean outward flow that might affect the turbulence parameters like u_{rms} and L_I in the otherwise cold non-reacting flow. It appears that in most experimental efforts on turbulent expanding flames, only cold flow turbulence parameters like u_{rms} and L_I measured in the absence of flame have been reported [7–12] with the exception of Lawes [13] who performed one point Laser Anemometry in the fresh mixture ahead of the turbulent flame. It is thus critical to investigate with detailed field measurements, to what degree these fundamental quantities are affected, if at all, by the flame as these modified parameters are what distort the flame instead of the quantities measured in its absence.

In view of such a need, we shall attempt to provide experimental high-speed particle image velocimetry data that quantifies flame–turbulence interaction dynamics well resolved in two dimensional space and time, as the flame evolves from a wrinkled flame kernel to a well-developed expanding turbulent flame. The high-speed Mie scattering which is a necessary precursor to HS-PIV allows us to extract the flame edges from the maximum seed density gradients. This enables tracking the evolution of the stretch rates, curvature statistics. The flow velocity and strain rate tensor components from the HS-PIV could be superposed on these flame edges, allowing investigation of the evolution of stretch rate statistics due to both local strain rate and curvature.

2. Experimental method

The experiment uses a constant-pressure, dual-chamber, fan-stirred vessel that enables investigation of spherically expanding flames (Fig. 1a) with the help of high speed imaging. The chamber has been widely used for both laminar and turbulent expanding flames and is detailed in previous articles [1,9,19] and in the Supplementary material [S1].

To detect the flame edge during the combustion process the fuel/air mixture was seeded using DEHS droplets (nominal diameter 1–2 μm) using a high-pressure nebulizer. A high-speed Nd-YLF laser (527 nm) synchronized with a high-speed camera (Phantom v7.3) is used for Mie-scattering imaging and subsequent PIV processing. Using beam expanding optics the 2 mm diameter laser beam is expanded to a 750 μm thick laser sheet inside the inner chamber as shown in Fig. 1a. The camera placed at 90° from the laser plane recorded images with a pixel resolution of 608×600 to achieve a spatial resolution of ~50 μm/pixel. For high quality, high-speed 2D particle image velocimetry (PIV) the camera was triggered at a framing rate of 8000 frames/s with corresponding laser synchronization, such that the correlated image pairs could be recorded with a time interval of 30 μs. Before the ignition, the entire chamber remains filled with droplet mist showing a uniform distribution of seed density. Following ignition, as the flame propagates the seeding droplets vaporizes at the flame edge, hence limiting the high seeding density only outside of the flame.

Post processing was performed in two stages. First, from the high-speed Mie-scattering images the instantaneous 2D flame (on the laser plane) edge was detected using Canny edge detection technique through Matlab. Second, vector computation was performed using commercially available software DaVis multi-pass strategy with interrogation window size reducing from 16×16 to 8×8 pixel^2 having 50% overlap. Image area close to the electrodes was excluded from the vector calculation to minimize error. The consistency and accuracy of the vector computation was reflected in very high Q value (~0.95), which is the ratio of two most probable displacement values in each interrogation window. PIV was performed both in cold flow (before ignition) and with flame (after ignition). The information of instantaneous flame edge and velocity field was then combined onto a common grid to obtain the relevant flame–turbulence interaction statistics.

In the following we clarify the limitations and uncertainties of the technique used. The flame edge detected using Mie scattering images approximately represents an isotherm that corresponds to the boiling/saturation temperature of DEHS which is the composition of the seeding droplets. The resolution of the current high speed Mie scattering images is approximately 50 μm, which restricts us from completely resolving the finest structures for the very high pressure flames (Flame thickness and Kolmogorov length scales are tabulated in Table 1). Moreover, for PIV, the smallest interrogation window was 8x8 pixels

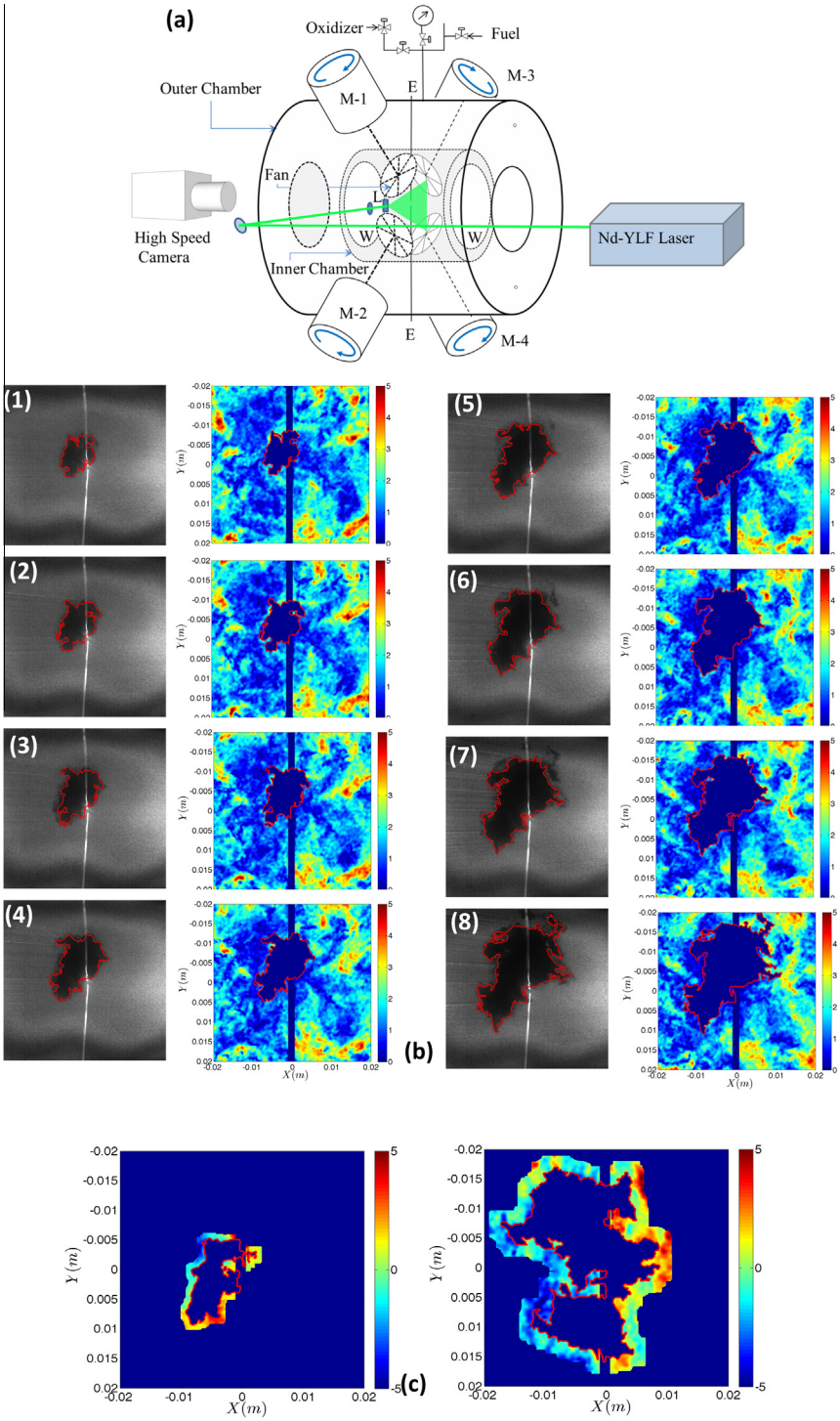

Fig. 1. (a) Experimental setup. (b) Instantaneous Mie-Scattering images and vector fields from one experiment (every alternate image has been shown here). The colormap in the vector field shows the magnitude of the local velocity field. The flame edge extracted from the Mie scattering image has been superposed on the vector field. (c) Two vector fields around the flame location. During post processing an artificial zone around the flame was identified to calculate the flow statistics and then compared with the flow statistics with no flame. The width of this zone was equal to the brush thickness of the flame. Thus, we see that the width of the zone increases with radius as the flame brush also increases. (For interpretation of the references to colour in this figure legend, the reader is referred to the web version of this article.)

Table 1
Experimental conditions and relevant parameters (ϕ: equivalence ratio, p_0: atmospheric pressure, Re_T: Turbulent Reynolds number $= (u_{rms}{*}L_I/\nu)$, ν: kinematic viscosity of unburned gas. S_L: Planar laminar flame speed, $S_{L,b}$: Planar laminar flame speed on burned side, δ_L: Laminar flame thickness, η: Kolmogorov microscale, Mk_b: Markstein number on burned side, Da: Damkohler Number $= (L_I/u_{rms}){*}(S_L/\delta_L)$).

Mixture	ϕ	p/p_0	rpm	u_{rms} (m/s)	Re_T	S_L (m/s)	$S_{L,b}$ (m/s)	δ_L (m)	η (m)	Mk_b	Da
CH_4–air	0.90	1	2000	1.29	328	0.32	2.31	4.80E-04	4.85E-05	1.18	1.88
CH_4–air	0.90	1	4000	2.57	656	0.32	2.31	4.80E-04	2.89E-05	1.18	0.94
CH_4–air	0.90	2	2000	1.29	656	0.25	1.83	2.90E-04	2.89E-05	1.06	2.41
CH_4–air	0.90	2	4000	2.57	1312	0.25	1.83	2.90E-04	1.72E-05	1.06	1.21
CH_4–air	0.90	5	2000	1.29	1641	0.17	1.22	1.60E-04	1.45E-05	0.73	2.97
nC_4H_{10}–air	0.80	5	2000	1.29	1641	0.18	1.18	1.27E-04	1.45E-05	2.75	3.96

with 50% overlap (1 vector every 4×4 pixels), hence further reducing resolution of the data.

3. Results and discussion

In this work we have studied the expanding flame in a near-isotropic turbulent flow field for two fuels at three different pressures and two different turbulent intensities. The full list of the experimental conditions and relevant parameters are given in Table 1. The Lewis numbers of all the operating conditions are close to or greater than 1 diminishing any chances of diffusional thermal instability. Within the conditions of interest, Darrieus–Landau instability was absent as well. The Markstein numbers (Mk) obtained from laminar expanding flame experiments for the CH_4–air mixture conditions corresponding to the turbulent experiments of interest slightly decreases with pressure from 1.18 to 0.73.

3.1. Flow statistics

In Fig. 1b evolution of the flame edge for CH_4-air $\phi = 0.90$ flame at low turbulence intensity ($u_{rms} = 1.29$) at pressure $p = 1$ atm, is shown. To extract the influence of the flame on the flow, a zone of specified thickness (the standard deviation of flame edge radial position distribution, or the brush thickness) was defined around the flame as shown in Fig. 1c to perform the statistical evaluation. Figure 2a and b show the mean radial velocity $\langle U_r \rangle$ and the effective turbulent intensity on the flame $u'_{xy} = \left[\frac{1}{2}(\langle(u_x - \langle u_x\rangle_R)^2\rangle_R + \langle(u_y - \langle u_y\rangle_R)^2\rangle_R)\right]^{1/2}$ for all the cases under study, respectively. It is noted that the value of u'_{xy} is independent of axes orientation. We also compared these results with those obtained from the corresponding cold flow measurements in the absence of flame, prior to ignition. It is to be noted that the above revised definition w.r.t. our previous work [9] and new HS-PIV data yielded a new correlation between effective rms of fluctuating velocity (m/s), fan speed (rpm) and radius (m). This new correlation is $u'_{xy} = 0.002339(\text{rpm})\langle R\rangle^{0.33}$. We observe that in the absence of the flame the mean radial flow is directed inward (towards the center of the chamber) indicated by the negative values in Fig. 2a. This weak radial flow also increases with radius, closer to the fans. However during flame expansion, the mean radial flow adjacent to the flame is radially outward in nature shown by the positive values of $\langle U_r \rangle$. As the flame expands it pushes the unburnt gas in front of it. This effect becomes stronger as the flame accelerates with increase in radius, resulting in increasing $\langle U_r \rangle$ with $\langle R \rangle$. However, we found that there is no discernible change in the u'_{xy} in the presence of the flame. This shows the effect of flame on turbulence intensity is rather weak in agreement with the experiments by Lawes [13].

In Fig. 3 we look into the evolution of the probability distribution functions (*pdf*s) for K_t and K_n defined in Eq. (2). The *pdf*s are computed over the ensemble of all the runs for a given condition, conditioned at particular values of $\langle R \rangle$. It is clearly seen that both the K_t and K_n show self-similar profiles during their evolution with $\langle R \rangle$. However, when plotted on a log scale the nature of the *pdf* tails of K_t and K_n appear different. The *pdf* for K_t shows parabolic tails suggesting Gaussian distribution, whereas K_n shows non-Gaussian stretched tails implying finite probability of very large K_n values in comparison to its near Gaussian counterpart K_t. Clearly with increase in fan speed or u_{rms} both the K_t and K_n *pdf* tails are flared. As the turbulence Reynolds number Re_T increases (with turbulence intensity), the Kolmogorov length scale η decreases, resulting in the emergence of smaller scale eddies which are also highly strained and intermittent. These impart larger K_t and K_n observed from the flaring of the tails. It is also important to see if the increased u_{rms} or Re_T has similar impact on the mean stretch rates in addition to that on the higher moments. In Fig. 4a and b, $\langle K_t \rangle$ and $\langle K_n \rangle$ are plotted vs. $\langle R \rangle$ for all conditions of interest. In Fig. 4a we find

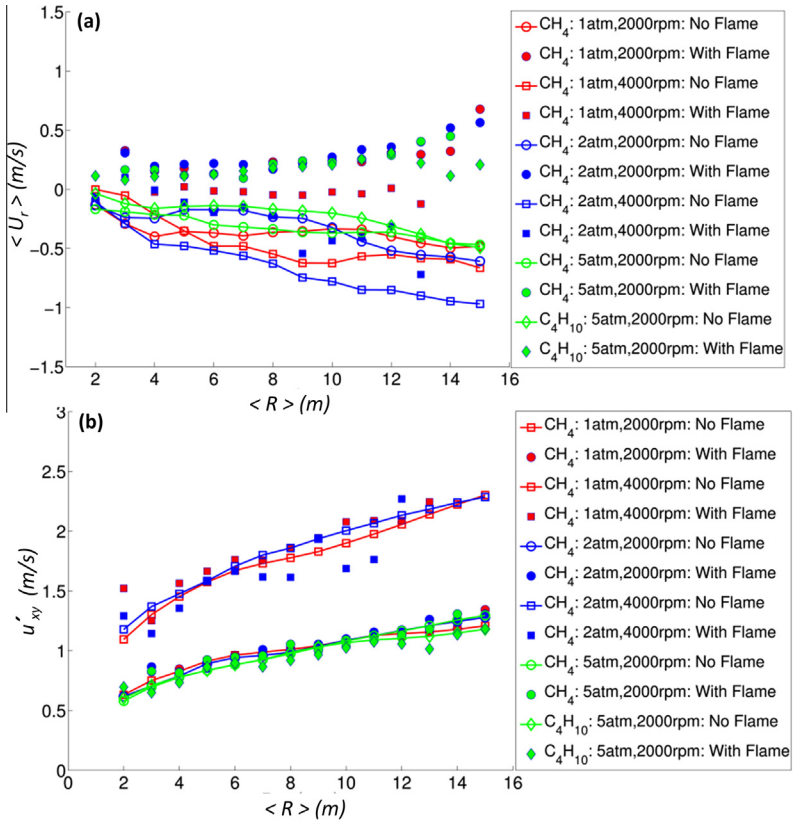

Fig. 2. Plot of (a) ensemble averaged $\langle U_r \rangle$ vs. $\langle R \rangle$ and (b) ensemble averaged u'_{xy} vs. $\langle R \rangle$ in presence and in absence of flame.

that the $\langle K_t \rangle$ magnitudes are weakly positive over the entire range of $\langle R \rangle$ for all conditions. It was proven in [20,21] that material surfaces in isotropic turbulence must experience positive $\langle K_t \rangle$. Since propagating surfaces do not perfectly follow the flow, identical behavior is not guaranteed for premixed flames. Though for low Damköhler number (Da) flames, positive $\langle K_t \rangle$ is expected, as has been shown in [22–23]. Interestingly, we find that $\langle K_t \rangle$ progressively decreases with $\langle R \rangle$, which might be attributed the acceleration of the mean flame surface, thus providing shorter residence times to the turbulent eddies to impart tangential strain. The normal strain $\langle K_n \rangle$ is also mostly positive over $\langle R \rangle$ but with relatively higher degree of scatter. However, contrary to the observation in Fig. 3 where increasing u_{rms} and Re_T resulted in a discernible change in *pdf* shapes especially at their tails, the ensemble averages of Fig. 4 hardly show any variation with the changes of the above parameters. For all conditions in the current study $\langle K_t \rangle$ and $\langle K_n \rangle$ vs. $\langle R \rangle$ profiles appear invariant. The normal strain, $K_n = (\mathbf{v} \cdot \mathbf{n})\kappa$, controlled by flame curvature and flow velocity normal to the flame surface, appears to be almost constant, although the flame curvature decreases with flame radius. This is primarily caused by increase in the mean flow velocity normal to the flame due to the mean flame acceleration combined with gas expansion (Fig. 2a). These opposing effects could result in the near constant profile of K_n.

3.2. Persistence time scales

Recently Clavin and Graña-Otero [24] analytically showed the existence of two unique Markstein lengths, one due to strain rate and the other due to curvature. Following the same notion, if one can isolate the persistence time scales of these two Markstein lengths, it is possible to distinguish between their relative importance and to assess the relative relevance of local strain and local curvature for dissipating turbulent flame surface fluctuations. From a modeling point of view this is of considerable interest especially in the context of G-equation used for the description of a premixed flame [25,26]. Currently, to describe the response of flame speed to unsteady stretch, expected in turbulent flows, two limiting conditions are typically used. The first approach is to consider Markstein lengths obtained in steadily

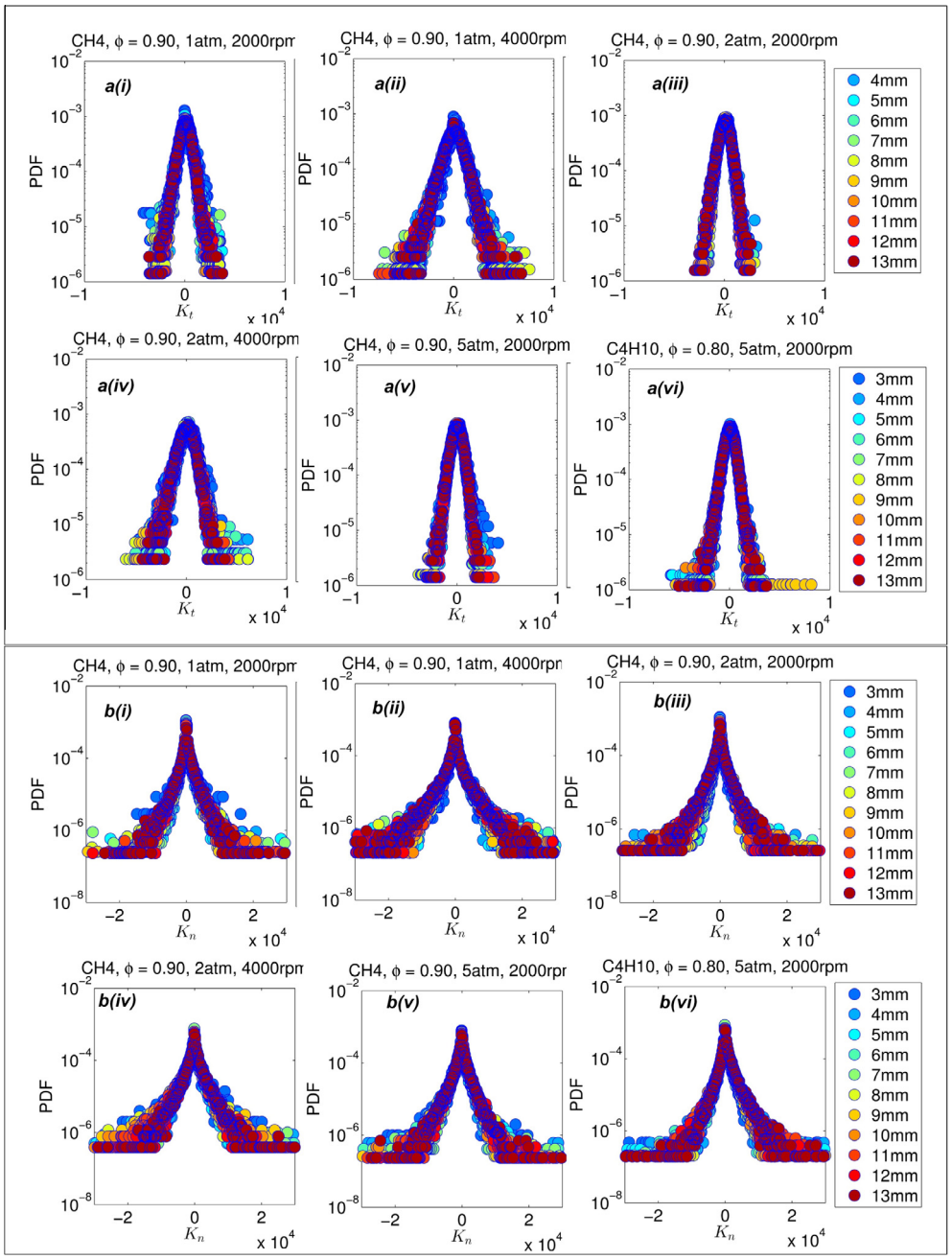

Fig. 3. (a) PDFs of K_t and (b) PDFs of K_n conditioned at specific values $\langle R \rangle$, over six different conditions of fuel–air mixtures, u_{rms} and pressure: (i) CH_4: 1 atm and 2000 rpm, (ii) CH_4: 1 atm and 4000 rpm, (iii) CH_4: 2 atm and 2000 rpm, (iv) CH_4: 2 atm and 4000 rpm, (v) CH_4: 5 atm and 2000 rpm, (vi) C_4H_{10}: 5 atm and 2000 rpm.

stretched flames [26] and the second approach is to consider vanishing effect of Lewis number (Le) under overwhelming presence of turbulent transport say in thickened flamelet regimes [25]. It is possible that for wide conditions of interest in moderate to large turbulence Reynolds numbers ($Re_T > 100$) and intermediate Damköhler numbers ($0.1 < Da < 10$) the flame response to stretch is somewhat intermediate. However, there is little systematic study on this topic, with the exception of the analytical work by Clavin and Joulin [27], although the conditions there may not be directly relevant for turbulent flows. We attempt to address this problem by following/

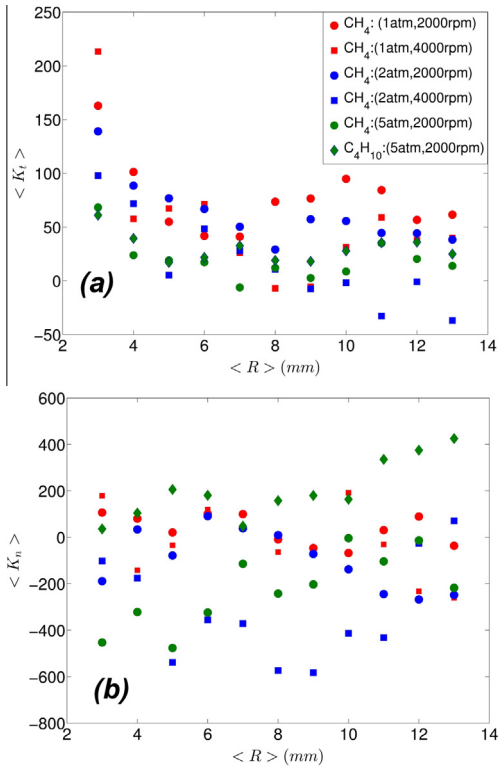

Fig. 4. (a) $\langle K_t \rangle$ and (b)$\langle K_n \rangle$ vs.$\langle R \rangle$ for all experimental conditions.

tracking specific points on the flame surface, by displacing them with the vector sum of their local flame speeds in the surface normal direction and local flow velocities. A surface point on a reacting isosurface defined as a flame particle has been recently studied using DNS [28]. The stretch time history that a flame particle carries can be directly used to answer fundamental questions of broader practical relevance like turbulent flame speed, flame extinction, etc. It is to be noted that since we only have velocity and flame surface information in a 2D plane, we can only track the motion of an edge point that is constrained to remain on the 2D plane. Adopting the definition and notation of Pope for surface points [29], the motion of such in-plane flame particle can be described by:

$$\frac{d}{dt}\mathbf{X}^F_{2D}(t) = \mathbf{U}_{2D}\left(\mathbf{X}^F_{2D}[t],t\right) + S_d\left(\mathbf{X}^F_{2D}[t],t\right)\mathbf{n}^F_{2D}\left(\mathbf{X}^F_{2D}[t],t\right). \quad (3)$$

Here $\mathbf{X}^F_{2D}$ is the position vector of the flame particle on the flame edge at time t. The local displacement flame speed could be modeled as $S_d = S_L - \delta_M \mathbf{K}$, with δ_M obtained from laminar expanding flame experiments. Figure 5a and b show the time evolution of the flame edges colored with local tangential strain rates K_t and stretch rate due to pure curvature K_c, respectively for CH_4-air 1 atm 2000 rpm flame condition. Figure 5c and d show the corresponding images

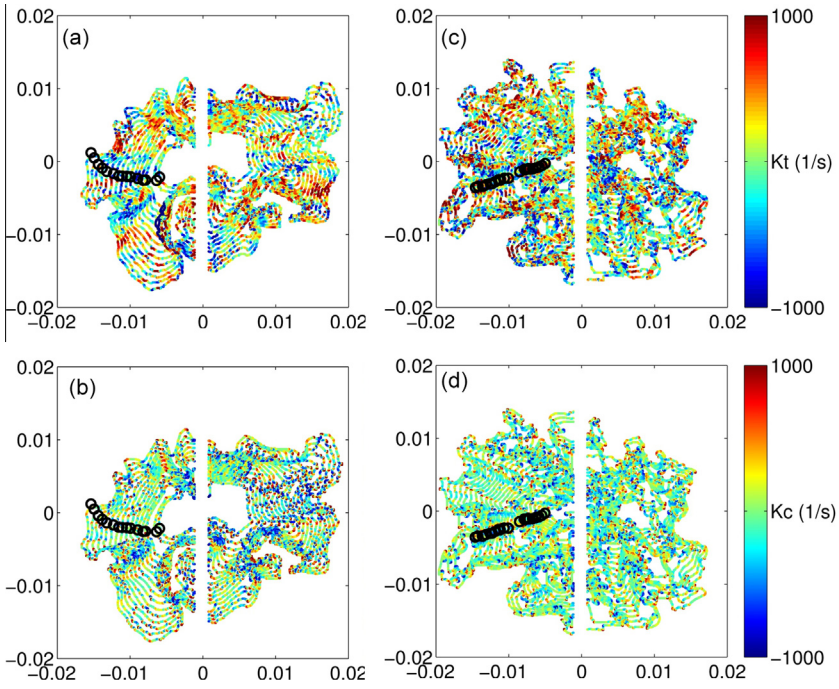

Fig. 5. Evolution of flame edge with time, colored by (a) K_t (b) K_c for CH_4-air $\Phi = 0.9$, 2000 rpm, $p = 1$ atm; flame edge colored by (c) K_t (d) K_c for C_4H_{10}-air $\Phi = 0.8$, 2000 rpm, $p = 5$ atm. (For interpretation of the references to colour in this figure legend, the reader is referred to the web version of this article.)

for the C_4H_{10}–air, 5 atm, 2000 rpm case. The path tracked by a representative flame particle is shown by black circles. On the first frame the flame particles are positioned on each of the flame edge points and are allowed to evolve according to Eq. (3). Since the edge is located only at discrete points on the grid, it might happen that the flame particles do not land up exactly on the edge at the subsequent instant. In that case the edge point, which is at the shortest distance from the new flame particle position, is considered to be the updated position. The K_t and K_c time histories from each flame particle are subsequently auto-correlated. The integral of the ensemble averaged autocorrelation function yields the integral time scale for K_t and K_c. These time scales are averaged over all the runs over the same conditions to yield the final persistence time scales τ_{P,K_t} and τ_{P,K_c} of K_t and K_c, respectively. For example:

$$\tau_{P,K_c} = \left\langle \int_0^{\infty} \frac{\overline{K_c\left(\mathbf{X}_{2D}^F[t],t\right)K_c\left(\mathbf{X}_{2D}^F[t+\tau],t+\tau\right)d\tau}}{var(K_c)} \right\rangle, \tag{4}$$

where the bar and angular brackets denote time and ensemble average, respectively. These are shown in Fig. 6 for all experimental conditions. We find that for all conditions under study τ_{P,K_t} remains rather invariant within a range of 400–600 μs. However, the τ_{P,K_c} shows a much higher degree of sensitivity in response to the change in u_{rms}, pressure and hence Re_T, and varies from about $\tau_{P,K_c} \sim 800\mu s$ for the CH_4, 1 atm, 4000 rpm case to about $\tau_{P,K_c} \sim 1.8ms$ for the C_4H_{10}, 5 atm, 2000 rpm case. In general considering all cases under study, the τ_{P,K_c} is greater than τ_{P,K_t} by nearly a factor of 2. This suggests that strain rate due to pure curvature might be a more persistent quantity than that due to tangential strain in the current configuration and conditions.

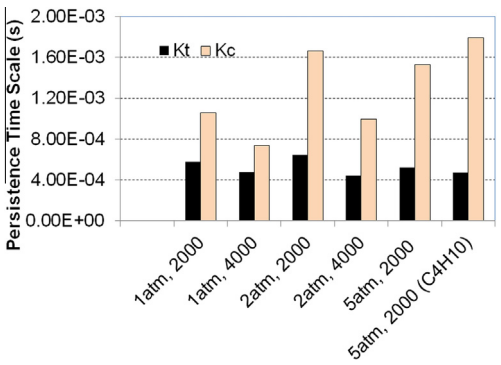

Fig. 6. Persistence time scales of K_c and K_t over all experimental conditions. CH_4-air was used in the first five cases.

Even without flame particle tracking, from Fig. 5 we qualitatively observe that the geometry of the flame edges remains correlated with the evolution in time for both cases. Local curvature being a measure of the local geometry thus quantitatively emerges as a rather persistent quantity for the flames under consideration. This experimental finding is in line with recent theoretical work by Clavin and co-workers [27], which suggested that the effect of curvature on flame propagation can be significantly higher than that of normal and tangential strains rates when both are fluctuating at high frequencies. In certain cases, of course, highly fluctuating (or uncorrelated) tangential strain can indeed intermittently affect the flame surface and, as a result, its evolution.

Though these persistence time scales are obtained from 2D flame particle tracking, it is to be recognized that experimentally tracking the motion in 3D is extremely challenging if not currently impossible, given the necessity of simultaneous volumetric imaging of flow and reactive isosurfaces with high time resolution. Hence the representative persistence time scale information of tangential strain rate and curvature gleaned from the 2D motion of the surrogate flame particle remains to be of substantial interest.

4. Conclusions

In summary, we report herein simultaneous high-speed measurements of flame location and velocity field in a turbulent expanding flame. This first of its kind measurement sheds light on flame–turbulence interaction though quantitative information about the evolution of flow fields adjacent to the flame surface and stretch rates on the flame. Experiments performed at multitude of pressure and fan speeds confirm that the expanding flame pushes the unburnt gases creating a mean radially outward flow at the vicinity of the flame. However effect of flame on the u'_{xy} of the nearby flow field is rather weak when compared with the local cold flow statistics. On the other hand, comparison of stretch rate *pdf*s, especially K_t and K_n, shows that the K_t follows a Gaussian distribution while the K_n follows a stretched Gaussian profile with long tails. The tails of the distributions are found to expand with the turbulent intensity (fan speed) as the smaller eddies become stronger to stretch the flames with a positive $\langle K_t \rangle$ for all cases under consideration.

Comparison of evolution of two principal stretch rate contributors, K_c and K_t, reveals the presence of two different persistence timescales that are relevant for the dissipation of flame surface fluctuations. The current study through 2D flame surface particle tracking method shows that the persistence/integral time scales associated with K_c is almost twice as that of K_t.

Acknowledgements

This work was supported by Air Force Office of Scientific Research under the technical monitoring of Dr. Chiping Li.

Appendix A. Supplementary data

Supplementary data associated with this article can be found, in the online version, at http://dx.doi.org/10.1016/j.proci.2014.07.038.

References

[1] A.P. Kelley, C.K. Law, *Combust. Flame* 156 (9) (1844) 2009.
[2] N. Peters, *Turbulent Combustion*, Cambridge University Press, NY, 2000.
[3] J.F. Driscoll, *Prog. Energy Combust. Sci.* 34 (2008) 91.
[4] A.N. Lipatnikov, J. Chomiak, *Prog. Energy Combust. Sci.* 36 (2002) 1.
[5] H. Pitsch, *Annu. Rev. Fluid Mech.* 38 (2006) 453.
[6] S.B. Pope, *Annu. Rev. Fluid Mech.* 19 (1987) 237.
[7] R.G. Abdel-Gayed, D. Bradley, M. Lawes, *Proc. Roy. Soc. London, A* 414 (1987) 389.
[8] D. Bradley, M. Lawes, M.S. Mansour, *Combust. Flame* 158 (2011) 123.
[9] S. Chaudhuri, F. Wu, C.K. Law, *Phys. Rev. E* 88 (2013) 033005.
[10] D. Bradley, M.Z. Haq, R.A. Hicks, et al., *Combust. Flame* 133 (2003) 415.
[11] M. Fairweather, M.P. Ormsby, C.G.W. Sheppard, R. Woolley, *Combust. Flame* 156 (2009) 780.
[12] M. Lawes, M.P. Ormsby, C.G.W. Sheppard, R. Woolley, *Combust. Flame* 159 (2012) 1949.
[13] M. Lawes, Effects of turbulence on combustion in engines, Ph.D. thesis (1987) University of Leeds.
[14] G.H. Markstein, *J. Aeronaut. Sci.* 18 (1951) 199.
[15] P. Pelce, P. Clavin, *J. Fluid Mech.* 124 (1982) 219.
[16] M. Matalon, B.J. Matkowsky, *J. Fluid Mech.* 124 (1982) 239.
[17] S.H. Chung, C.K. Law, *Combust. Flame* 55 (1984) 183.
[18] F. Creta, M. Matalon, *J. Fluid Mech.* 680 (2011) 225.
[19] G. Rozenchan, D.L. Zhu, C.K. Law, *Proc. Combust. Inst.* 29 (2002) 1461.
[20] W.J. Cocke, *Phys. Fluids* 12 (1969) 2488.
[21] S.A. Orszag, *Phys. Fluids* 13 (1970) 2203.
[22] T.A. Echekki, J.H. Chen, *Combust. Flame* 106 (1996) 184.
[23] N. Chakraborty, S. Cant, *Combust. Flame* 137 (2004) 129.
[24] P. Clavin, J.C. Graña-Otero, *J. Fluid Mech.* 686 (2011) 187.
[25] N. Peters, *J. Fluid Mech.* 384 (1999) 107.
[26] S. Chaudhuri, V. Akkerman, C.K. Law, *Phys. Rev. E* 84 (2011) 026322.
[27] P. Clavin, G. Joulin, *Combust. Theor. Model.* 1 (4) (1997) 429.
[28] S. Chaudhuri, *Proc. Combust. Inst.* 35 (2) (2015) 1305–1312. http://dx.doi.org/10.1016/j.proci.2014.08.007.
[29] S.B. Pope, *Int. J. Eng. Sci.* 26 (5) (1988) 445.